Phase Distribution in an Upflow Monolith Reactor Using Computed Tomography

M. H. Al-Dahhan and A. Kemoun
Washington University, Chemical Reaction Engineering Laboratory, Washington University, St. Louis, MO 63130

A. R. Cartolano
Air Products and Chemicals, Allentown, PA 18195

DOI 10.1002/aic.10665
Published online November 2, 2005 in Wiley InterScience (www.interscience.wiley.com).

Computed tomography (CT) is known to be a viable technique for determining flow maldistribution in two-phase flow through packed beds. In this study, gamma ray computed tomography has been used to quantify the flow distribution in a monolith catalytic bed, with water as the liquid phase and air as the gas phase, flowing co-currently upward. The flow conditions were selected to bracket some commercially viable operating conditions for such reactors. In the monolith core region, fairly uniform flow distribution has been obtained for all the flow conditions used. This distribution is quantified using the standard deviation of the holdup distribution. However, maldistribution of air and water in the monolith bed wall region due to wall effects at the monolith entrance has been observed and quantified by CT. The obtained results confirm that the entrance and exit regions of the monolith bed need to be carefully designed and to be free of obstacles and vortex creating devices. © 2005 American Institute of Chemical Engineers *AIChE J,* 52: 745–753, 2006

Keywords: monolith reactor, phase distribution, computed tomography, gas holdup, noninvasive measurements

Introduction

Fixed bed catalytic reactors are widely used in many industrial processes. Recently, structured packing elements (e.g., monoliths, and different structures such as "sandwich" and "open cross-flow" structures, etc.) have been suggested for various three-phase chemical processes (Harter et al., 2001; Jiang, 2000; Krishna, 1999, 2002; Marchot et al., 2001; Podrebarac et al., 1998). Monoliths have been successfully used in the automotive industry as catalytic converters for the abatement of NOx and CO emissions from engines (Cybulski et al., 1999; Cybulski and Moulijn 1998; Gulati, 1998; Roy et al., 2002) and in coal fired power plants for removing NOx from the flue gas (Beretta et al., 1998; Roy et al., 2002) via catalytic gas phase reactions. However, their potential for use in multiphase reactors has not yet been fully realized. Superior performance of monolith reactors over conventional three-phase reactors (e.g., slurry bubble columns, packed beds, and fluidized beds) has been demonstrated for a number of test reactions. Currently, Akzo Nobel produces hydrogen peroxide on a large scale using a monolith catalyst for the hydrogenation of anthraquinone to the corresponding hydroquinones (Albers et al., 2001). Moreover, monolith reactors offer low pressure drop and, hence, provide high throughput over these conventional pellet-based reactors. In addition, the small size of the channels in monoliths and the resulting small diffusion paths provide higher mass transfer compared to packed bed reactors. (Kreutzer et al., 2003; Liu, 2002; Liu et al., 2002; Mazzarino and Baldi, 1987; Nijhuis et al., 2001; Patrick and Abraham, 2000; Roy et al., 2002; Stankiewicz, 2001; Stankiewicz and

Correspondence concerning this article should be addressed to M. H. Al-Dahhan at muthanna@che.wustl.edu.

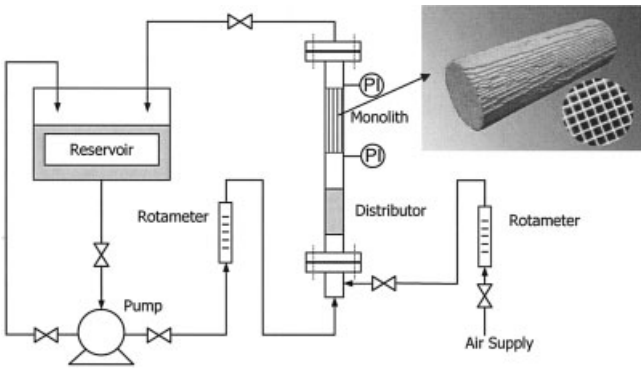

Figure 1. Monolith structure and the monolith reactor flow setup.

Moulijn, 2000). Recently, Roy et al. (2002), after fundamental modeling of the transport-kinetic interactions in a monolith catalyst, proposed a methodology to optimally design the monolith geometry and select the operating conditions for given gas-liquid-solid reactions to be used with monolithic catalysts in new reactors or in retrofit designs.

Monoliths consist of a large number of thin parallel channels, as shown in Figure 1. The cross sections can be squares, triangles, or other geometrical shapes. To increase the surface area and enhance the mixing and phase interactions, fins can be added inside each channel. The number of channels per unit cross section is the "cell density," commonly defined as channels per square inch (cpsi). Typically, cell density ranges between 100 and 1200 cpsi (Gulati, 1998; Roy et al., 2002).

Gas-Liquid flow monolithic reactors can be operated in batch or continuous modes. In batch mode, the liquid phase is circulated through the monolith unit while the gas phase flows in one pass until the desired conversion is achieved. In continuous mode, both liquid and gas flow once through the monolith unit. In either mode, liquid and gas can flow either counter-currently, co-currently upward, or co-currently downward. Different distributor configurations can be used to distribute gas and liquid phases uniformly into the monolith channels. These configurations include a spray nozzle, showerhead, ejector, mesh structure, plate with holes, sintered plate, and static mixer. Since the channel walls prevent radial mixing inside the monolith beds, the initial gas and liquid distribution is critical for the desired performance. The monolith reactor can be operated in either Taylor flow (slug flow) or annular flow regimes. The Taylor flow regime is characterized by a train of liquid slugs followed by gas bubbles moving consecutively through the channels. In this flow regime, which is desirable for enhanced mass transfer, the gas bubbles' length is several times larger than the channel diameter, and their diameter is almost equal to the channel diameter. A very thin liquid film separates the gas phase from the channel wall. Typically, the liquid film thickness is in the range of 30 to 70 μm (Irandoust et al., 1989). By comparison, the annular flow regime is characterized by the flow of liquid along the channel wall as a thick film, and the gas phase is in the core of the channel. This regime can be obtained at low liquid and high gas flow rates.

Properly understanding the hydrodynamic parameters and flow distribution in monolith reactors is essential for their successful design, scale-up, and operation. Gas/Liquid holdup and their cross-sectional distribution are important hydrodynamic parameters. Due to the complex nature of the interaction between gas, liquid, and solid phases, one of the major challenges in the design and operation of these types of reactors is achieving a proper flow distribution. Maldistribution of either the gas or the liquid phase can cause hot spots, reactor runaway for exothermic reactions, decreased selectivity to desired products, and underutilization of the catalyst. Although monolith reactors have recently emerged as an attractive alternative for three-phase reactor applications, hydrodynamic studies, particularly of the gas-liquid flow distribution, are scarce. A few studies have measured overall gas/liquid holdup and pressure drop in monolith reactors using various techniques (Harter et al., 2001; Mewes et al., 1999).

Most of the investigations using monolith reactors have dealt with downflow gas and liquid phases, while some industrial applications may operate in co-current upflow mode. Unfortunately, these studies do not address the holdup distribution across the monolith bed, which is a direct result of the gas-liquid flow distribution at the entrance of the bed. Because the monolith bed is opaque, optically based non-invasive techniques, such as digital particle image velocimetry (DIPV) and laser doppler anemometry (LDA), cannot measure the liquid/gas holdup distribution over its cross-section.

Recently, different types of non-invasive tomographic techniques have been used to measure holdup distribution in packed-beds. These techniques include gamma-ray computed tomography (Boyer and Fanget, 2002; Chen et al., 2001; Harter et al., 2001; Wang et al., 2001; Yin et al., 2002), X-ray tomography (Lutran et al., 1991; Schmit et al., 2000, 2001; Toye et al., 1996, 1998), and electrical capacitance and resistance tomography (Mewes et al., 1999; Reinecke and Mewes, 1996; Reinecke et al., 1998). The use of nuclear magnetic resonance imaging (MRI) to visualize dynamic two-phase flow in monolith channels has been demonstrated by Mantle et al. (2002) and Heibel et al. (2001), but the flow conditions studied were essentially trickle flow.

In general, however, the holdup distribution in structured packing beds has not been fully investigated using non-invasive techniques. Toye et al. (1998) and Marchot et al. (2001) investigated the holdup distribution using x-ray tomography in a 0.6 m diameter bed packed with corrugated sheet structured packing and operating in counter-current mode. Mewes et al. (1999) and Reinecke et al. (1996, 1998) have implemented electrical capacitance tomography to measure holdup distribution in monolith beds. In these beds, water was fed into the reactor downward with no gas phase flow, or both gas and liquid phases flowing downward.

It is obvious that holdup distributions in fixed structured bed reactors using non-invasive techniques need to be further investigated at relevant design and operating conditions.

The present work used gamma ray computed tomography (CT), developed at the Chemical Reaction Engineering Laboratory (CREL)–Washington University and used extensively to measure time averaged holdup distribution in various types of multiphase reactors (Chen et al., 2001; Kumar, 1994; Rammohan, 2002; Roy et al., 2002). The CT equipment was first validated for a 1.9 inch (0.048 m) monolith bed and then used

Table 1. Range of Liquid and Gas Flow Rates Used to Achieve Taylor Flow Regime (Includes the Flow Rates Used to Bracket the Industrially Interesting Flow Conditions U_L = 0.4 m/s and U_G = 0.4 m/s)

U_L (m/s)	U_G (m/s)	Q_L (GPM)	Q_G (SCFH)
0.3	0.3	4.6	39.3
0.4	**0.4**	**6.2**	**54.1**
0.4	0.3	6.2	40.6
0.3	0.4	4.6	53.1
0.3	0.5	4.6	64.7
0.5	0.3	7.7	41.4
0.4	0.5	6.2	66.0
0.5	0.4	7.7	52.8
0.5	0.5	7.7	66.0

to study the holdup distributions in such a bed with the air and water phases flowing co-currently upward. The flow conditions were selected to achieve the Taylor flow regime within the monolith channels.

Experimental Setup

Monolith reactor flow system

The monolith setup, shown in Figure 1, consists of a monolith section, distributor, and liquid and gas delivery systems. Gas and liquid flow co-currently upward. The monolith was made of cordierite, with a diameter of 1.9 inches (0.048 m), a length of 6.0 inches (0.152 m), and cell density of 400 cells per square inch (cpsi). The monolith was fixed inside 5 cm clear PVC pipe. Hence, there was a small gap (~0.001-0.002 m) between the column wall and the monolith. The flow channels were of square cross section and measured nominally 1 mm along each side. The overall open area was calculated to be $12.5 \times 10-^4$ m^2. The monolith section was fixed inside the pipe using two Teflon gaskets, 0.0508 m (2 inches) in diameter and 0.004 mm wide, one at the top and another at the bottom of the monolith bed. The gaskets were held in place by support rings at the top and bottom, which held the bed in compression. This gasketing was used to eliminate bypassing of the bed to the outside, which reduced the functional diameter of the monolith to 0.0432 m (1.7 inches) and the area available to the flow to 9.72×10^{-4} m^2.

Water was the liquid phase. The liquid delivery system consisted of a feed tank, a pump, and a rotameter. Water was recycled by a centrifugal pump, as well as added if necessary, to maintain a constant suction head at the pump. The rotameter was calibrated at a constant static water level in the tank. The flow rate reading was also corrected with a coefficient related directly to the pressure at the monolith entrance. The in-house air system was used as the gas delivery system. Air entered the setup at a point below the distributor, which was mounted below the monolith section. The distributor was designed and selected to provide even mixing and breakup of gas bubbles before entering the monolith section. Two taps were mounted at the inlet and outlet of the monolith section for pressure and pressure drop measurements.

Experimental conditions

Table 1 shows the range of volumetric gas (Q_G, SCFH) and liquid (Q_L, GPM) flow rates selected to achieve Taylor flow regime (superficial liquid and gas velocities are denoted as U_L (m/s) and U_G (m/s), respectively), which includes the conditions bracketing commercially interesting flow conditions (U_L = 0.4 m/s and U_G = 0.4 m/s).

For all the conditions listed in Table 1, CT scans were performed at one axial level situated at the mid-height of the monolith (i.e., 0.0762 m above the entrance). In addition to the CT scans, validation experiments were performed with an empty monolith bed for porosity measurement. For gross maldistribution measurement, CT scans were made with half of the monolith filled with water and the other half empty and sealed at both ends.

One additional experiment, at U_L = 0.3 m/s and U_G = 0.36 m/sec, was performed without the supporting Teflon gaskets to illustrate its effect on the backmixing at the inlet and outlet of the monolith. The backmixing results primarily from the holddown rings, as will be discussed later.

CT Facility and Measurement Procedure

Single source gamma ray computed tomography (CT) was used in this work to determine the time-averaged cross-sectional variation of the gas/liquid holdups at the operating conditions outlined earlier.

CT Facility

The CT used in this study is based on a third generation fan-beam configuration developed at the Chemical Reaction Engineering Laboratory (CREL). Details of the hardware and software have been described in previous work (Kumar, 1994; Kumar et al., 1995, 1997a,b). The key system elements are illustrated in Figure 2. The CT consists of an array of NaI detectors with a diameter of 0.0508 m (2 inches) and an encapsulated ~85 mCi Cs^{137} source located opposite to the center of the array of detectors. Three detectors were used in the present study to cover the cross section of the 0.0508 m diameter column. The detectors and the source are mounted on a plate, which is rotated 360 degrees around the axis of the column by a stepping motor that is controlled through a microprocessor. Moreover, the whole assembly can be moved in the axial direction along the column to scan different axial levels of the column. The source collimator provides a fan beam of 40 degrees in a horizontal plane, which is further collimated using $0.2 \times 0.1 \times 0.1$-m lead bricks with a central slit. Using a detector side collimator, which is controlled by another stepping motor, increases the number of projection measurements per detector. The motor moves this collimator along the arc defined by the detector-array, which is tantamount to using many small detectors as opposed to a few large ones. The collimator is made of lead and has a depth of 0.064 m and a height of 0.076 m, so the detectors are completely shielded by the collimator. Rectangular slots having dimensions of 0.002 m $\times$ 0.01 m are located in front of each detector for collimating and sampling the beams. The dimensions of these slots were optimized based on the consideration of providing adequate area for detecting photons with good statistics in the chosen sampling time (Kumar, 1994).

Modifications have been made on the detector/source collimators' configuration to improve CT spatial resolution to 0.002 m in the horizontal direction and 0.005 m in the vertical direction and on the stability of the angular movement of the detector/source plate.

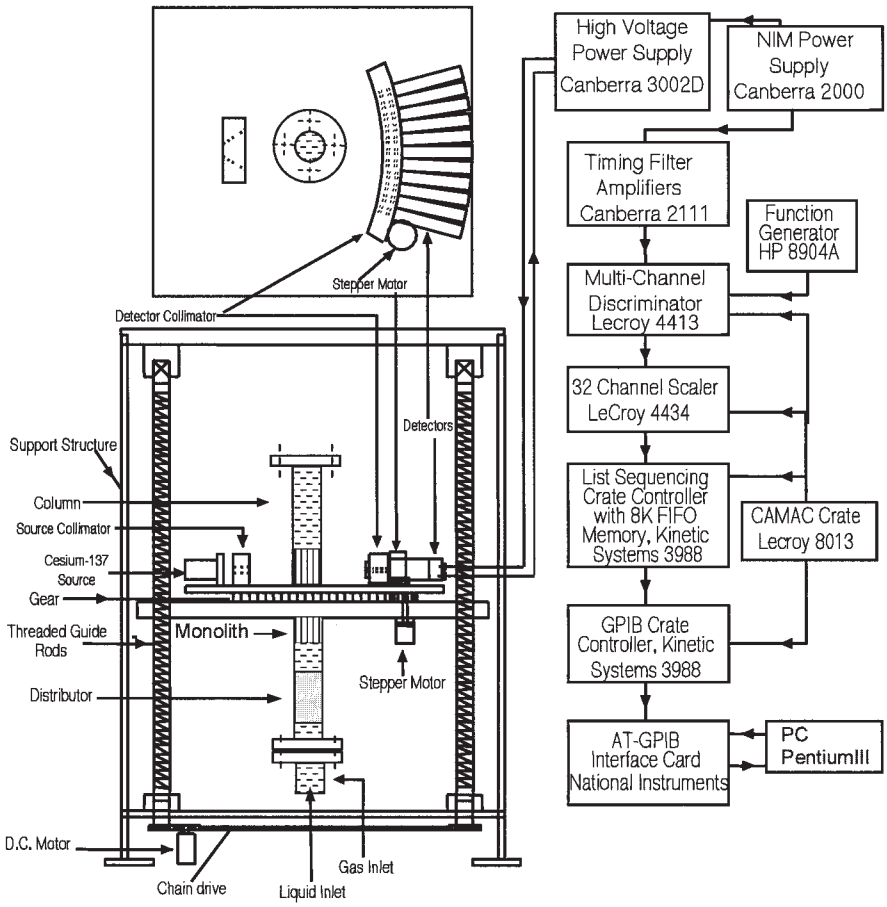

Figure 2. Single source CREL computed tomography (CT) setup.

Measurement procedure

The beam attenuations were measured along a number of beam paths through the column, originating from different angles. Based on Bear-Lambert's law, the intensity of a beam that is transmitted through a homogeneous material is expressed as follows:

$$T = \frac{I}{I_o} = e^{-\rho\mu\ell} \tag{1}$$

where T is the transmission ratio, I_o is the incident radiation, I is the detected radiation, μ is the mass attenuation coefficient, ρ is the medium density, and ℓ is the path length through the medium.

The measured $\ln(I_o/I)$ (called A, for simplicity) is equal to the integral sum of the attenuation through the material along the beam path.

$$A = \ln(I_o/I) = \rho\mu\ell \tag{2}$$

For computed tomography, attenuations are measured by the detectors along a number of such beam paths through the object from different directions around it. To reconstruct the holdup, the cross-section of the column is configured inside a square whose sides are equal to the column diameter. This square is divided into a number of square pixels.

Given a set of attenuation measurements by the detectors, the attenuation in each pixel (i.e., A_{ij}) can be obtained (reconstructed) by using a reconstruction algorithm. In this work, the estimation-maximization (E-M) algorithm was used (Kumar, 1994). Once A_{ij} for all pixels was obtained, image reconstruction of the holdup of the two phases was estimated according to Chen et al. (2001).

The E-M reconstruction algorithm was used for several reasons (Kumar, 1994): (1) it accounts for statistical variations associated with radiation measurements, (2) it readily incorporates non-uniform beam effect, and (3) it ensures that the final reconstruction will contain positive values. To obtain statistically significant results and to reduce the effect of position, the CT scans were obtained by scanning 360 degrees around the column for a total scanning time of about two hours.

If the scanned cross-section is divided into pixels (or cells) denoted by index ij, and if the medium is made of three materials with mass attenuation coefficients μ_g, μ_ℓ, and μ_s, densities ρ_g, ρ_ℓ, and ρ_s, and thicknesses ℓ_g, ℓ_ℓ, and ℓ_s, for the gas, liquid, and solid phases, respectively, then the total attenuation $A_{g-1-s,ij}$ is:

$$A_{g-1-s,ij} = \rho_g \mu_g \ell_{g,ij} + \rho_\ell \mu_\ell \ell_{\ell,ij} + \rho_s \mu_s \ell_{s,ij}$$
$$L = \ell_g + \ell_\ell + \ell_s, \quad \ell_{g,ij} = \varepsilon_g L_{ij}, \ \ell_{\ell,ij} = \varepsilon_\ell L_{ij}, \ \text{and} \ \ \ell_{s,ij} = \varepsilon_s L_{ij}, \tag{3}$$

where ε_g, ε_ℓ, and ε_s are the holdups (volumetric fractions) for the gas, liquid, and solid phases, respectively, and L_{ij} is the length of the pixel through which a particular gamma ray beam passes. Since the summation of the holdups equals unity (i.e., $\varepsilon_g + \varepsilon_\ell + \varepsilon_s = 1$) in each pixel, the attenuation of the CT scan for a three-phase system (Eq. 3) can be written as follows:

$$A_{g-\ell-s,ij} = \lfloor \rho_g \mu_g \varepsilon_{g,ij} + \rho_\ell \mu_\ell (1 - \varepsilon_{g,ij} - \varepsilon_{s,ij}) + \rho_s \mu_s \varepsilon_{s,ij} \rfloor L_{ij} \tag{4}$$

It is known that with a single-source CT, one can quantify the individual phase holdup distribution only for a two-phase flowing system. For a system with three moving phases, a dual source CT is needed. However, for a fixed bed, one can still use a single-source CT to measure the holdup distribution of the fixed solids phase ($\varepsilon_{s,ij}$) and then of the two flowing phases by using additional CT scans of the same column at the following conditions (Chen et al., 2001):

(i) The same column, but containing liquid only. Here, the attenuation of the same pixel beam (Eq. 4) is

$$A_{\ell,ij} = \rho_\ell \mu_\ell L_{ij} \tag{5}$$

(ii) The same column, containing gas and solids. In this case, the attenuation of the same pixel beam (Eqs. 4 and 5) is

$$A_{g-s,ij} = \lfloor \rho_g \mu_g (1 - \varepsilon_{s,ij}) + \rho_s \mu_s \varepsilon_{s,ij} \rfloor L_{ij} \tag{6}$$

(iii) The same column, containing liquid and solids. The attenuation of the same pixel beam (Eqs. 4, 5, and 6) is

$$A_{\ell-s,ij} = \lfloor \rho_\ell \mu_\ell (1 - \varepsilon_{s,ij}) + \rho_s \mu_s \varepsilon_{s,ij} \rfloor L_{ij} \tag{7}$$

Since $\rho_g \ll \rho_\ell$ or ρ_s, and μ_g, μ_ℓ, and μ_s are of the same order of magnitude, the attenuation caused by the gas phase is negligible. Hence, combining Eqs. 5, 6, and 7 yields the solids holdup in pixel *ij*:

$$\varepsilon_{s,ij} = 1 - (A_{\ell-s,ij} - A_{g-s,ij})/A_{\ell,ij} \tag{8}$$

By combining Eqs. 4, 5, 6, 7, and 8, an estimation of the local gas holdup in pixel *ij* can be obtained as follows:

$$\varepsilon_{g,ij} \equiv (A_{\ell-s,ij} - A_{g-\ell-s,ij})/A_{\ell,ij} \tag{9}$$

Thus, liquid holdup in pixel *ij* is calculated from

$$\varepsilon_{\ell,ij} = 1 - \varepsilon_{g,ij} - \varepsilon_{s,ij} \tag{10}$$

In order to maintain the same quality of the solids phase in all experiments, the monolith bed was first soaked in the liquid phase to fill the pore of the monolith walls with the liquid phase. Then the liquid was drained prior to scanning the bed for the cases listed above.

Evaluation of (I/I_o) for dry monolith scans from the measured (I/I_o) during the scans of monolith filled with liquid

As discussed in the previous section, scans of the monolith and air (i.e., step ii—the same column, containing gas and solids) are required to determine the distribution of gas and liquid in the monolith (or over the solids packing bed). When implementing CT on a large-scale pilot plant monolith random packed-bed reactor under operation, it is very difficult to dry the voidage to remove the stagnant liquid pockets/drops in order to scan the monolith in air (step ii). Hence, an attempt has been made and validated to estimate the (I/I_o) for the scans of monolith in air from the measured (I/I_o) during the scans of the monolith filled with liquid (step iii). The liquid-filled scan can be easily performed on large-scale pilot plant monolith beds. Such an approach was demonstrated on the lab-scale monolith unit discussed earlier and validated by comparing the estimated intensity counts (I/I_o) for monolith/air (step ii) with those experimentally measured.

Based on the steps discussed earlier and according to the Beer-Lambert law, the attenuation through the monolith (i.e., solids packing) and its walls filled with air and with water can be estimated by the following expressions:

$$\left(\frac{I}{I_0}\right)_{wall+mon+air} = e^{-(\rho_{air}\mu_{air}l_{air} + \rho_{monolith}\mu_{monolith}l_{monolith} + \rho_{wall}\mu_{wall}l_{wall})} \tag{11}$$

$$\left(\frac{I}{I_0}\right)_{wall+mon+water} = e^{-(\rho_{water}\mu_{water}l_{water} + \rho_{monolith}\mu_{monolith}l_{monolith} + \rho_{wall}\mu_{wall}l_{wall})} \tag{12}$$

Dividing Eq. 11 by Eq. 12 yields

$$\left(\frac{I}{I_0}\right)_{wall+mon+air} = \left(\frac{I}{I_o}\right)_{wall+mon+water} e^{-(\rho_{air}\mu_{air}l_{air} - \rho_{water}\mu_{water}l_{water})} \tag{13}$$

Since l_{air} and l_{water} are the same, and depend only on the view angle of the gamma ray projection, these can be geometrically determined as follows:

$$l_{cord} = 2\sqrt{R_c^2 - [(L_{\substack{source \\ column\_center}} + R_c)\mathrm{Sin}(\alpha)]^2} \cdot \sqrt{OPA} \tag{14}$$

Here R_c is the radius of the column, $L_{source,column\ \ center}$ is the distance from the center of the source to the center of the column, α is the angle between the gamma ray projections, and *OPA* is the open area of the monolith, which is taken as 60% of the monolith used in this work (as will be shown later).

In order to estimate $(I/I_o)_{wall+mon+air}$, we need to extract the following attenuation coefficient:

$$\rho_{equivalent}\mu_{equivalent} = \rho_{air}\mu_{air} - \rho_{water}\mu_{water}$$

The equivalent attenuation coefficient can be extracted from only one gamma ray projection, which passes through the center of the column and through the air and liquid used (here, water) separately. The equivalent attenuation coefficient value was found to be 8.10^{-4} for the water used in this study. This

value is then used to estimate the count projections for the scanned monolith/air step, with only l_{cord} as a geometric variable, as follows:

$$\left(\frac{I}{I_0}\right)_{wall+mon+air} = \left(\frac{I}{I_o}\right)_{wall+mon+water} e^{-(\rho_{equivalent}\mu_{equivalent}l_{cordal})l_{cord}} \quad (15)$$

Figure 3 shows that, using the above procedure, the computed scan counts in a monolith/air bed are within ±2% from the measured scan counts. The computed counts for the monolith/air for the laboratory-scale monolith are based on the measured counts during the scans of the monolith filled with water.

This validation is essential for the implementation of CT on a pilot plant-scale monolith, which accounts as well for all geometric irregularities at different views.

Results and Discussion

CT measurements were first validated by measuring the porosity distribution and averaged cross sectional porosity of the monolith by scanning the empty column and the column containing the monolith in air. The azimuthally averaged radial distribution of the measured porosity fraction was fairly uniform, with cross-sectional average of 0.61. The published value obtained from Corning, Inc., is 0.62 (here the porosity is defined as the ratio of the voidage volume to the total bed volume). The difference between the measured and published values of about ±2% is within the experimental error of the technique. This establishes confidence in the ability of our CT technique to properly capture the averaged bed structure.

To further validate the CT technique, a gross maldistribution was created by flooding half of the monolith bed with water, which was clearly detected by the CT scan.

Gas/Liquid distribution in the monolith

Figure 4 shows that at conditions of Q_L = 4.6 gpm (U_L = 0.3m/s) and Q_G = 39.3 SCFH (U_G = 0.3m/s), the gas/liquid distribution is fairly uniform across the inner part of the monolith cross-section. The gas holdup (ε_g), which is defined as the ratio of gas volume to the total reactor volume, as specified in

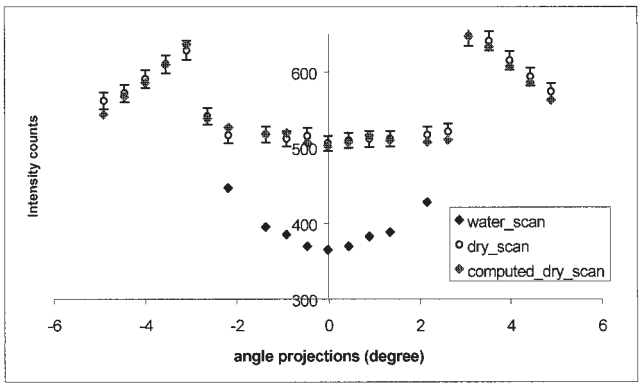

Figure 3. Comparisons of the computed dry-scan from the water scan against the experimental values obtained with a dry monolith done in the laboratory scale of 2-in. diameter.

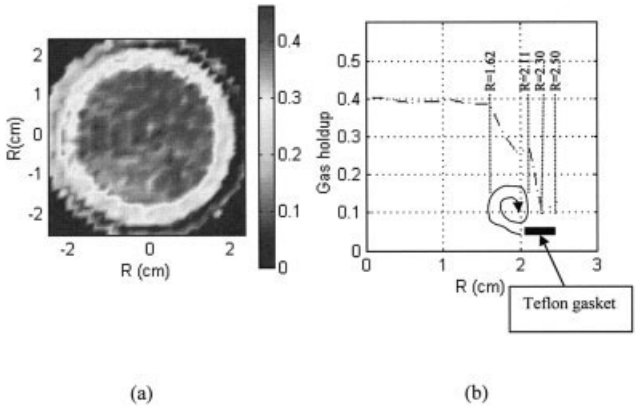

Figure 4. Gas holdup distribution at U_L = 0.3 m/s (Q_L = 4.6GPM) and U_G = 0.3 m/s (Q_G = 39.3SCFH).

(a) Time averaged cross-sectional gas holdup distribution; (b) azimuthally averaged gas holdup radial profile. The average gas holdup over the entire radius is 0.297, which is equivalent to gas saturation ($\varepsilon_g/(1-\varepsilon_s)$) of 0.48.

Eqs. 3 and 4, reaches about 0.4 in most of the channels. This means that the liquid holdup (ε_L) ($\varepsilon_L = 1 - \varepsilon_g - \varepsilon_s$) in the inner part of the monolith bed is equal to about 0.2, where solids holdup is about 0.4 (1-porosity fraction). However, the gas holdup drops from 40% to 25% between r = 0.64 inches and 0.83 inches (1.62 and 2.11 cm). It then drops significantly, from 25% to 10%, between r = 0.83 inches and 0.91 inches (2.11 m and 2.30 cm) and then increases slightly from 10% to 12%, between r = 0.91 inches to 0.98 inches (2.3 to 2.5 cm). In all these regions, the remaining volume is filled with solids (ε_s = 1 − porosity fraction) and liquid ($\varepsilon_L = 1 - \varepsilon_s - \varepsilon_g$). The decrease in gas holdup in the region between r = 0.64 inches (1.62 cm) and 0.83 inches (2.11 m) results from vortices, which were visually observed, at the entrance of the monolith due to a support ring. These vortices push the main axial two-phase flow to the center of the column, and caused coalescence of bubbles in this system, resulting in lower gas holdup in the annular region, as shown in all of the Figures. The decrease in the gas holdup in the annulus between the r = 0.83 inches (2.11 cm) and 0.91 inches (2.30 cm) is due to the use of the gasket at the inlet, as mentioned earlier. This decrease in gas holdup (ε_g) at the outer edge is due to the presence of stagnant liquid in the gap between the monolith and the column wall. The average gas holdup (ε_g) over the entire radius of Figure 4 is 0.297, which is equivalent to 0.48 gas saturation (gas saturation is the ratio of gas volume to the voidage volume ($\varepsilon_g/(1-\varepsilon_s)$).

Further evidence of stagnant liquid at the wall region due to the gasket is presented in Figure 5, where its radial profile is compared with that obtained without the gasket at similar flow rates. The gas holdup increased in the region previously occupied by the gasket, although some reduced gas holdup still exists near the wall. This reduction is due to bypassing of the monolith, caused by removal of the gasket, but impacted by the presence of the support ring.

Figure 6 shows the gas holdup distribution at the desired commercial flow conditions of U_L = 0.4m/s (Q_L = 6.2GPM) and U_G = 0.4m/s (Q_G = 54.1SCFH). Moreover, Figures 7 and 8 show examples of the gas holdup distribution at the conditions bracketing this flow condition. Here, the same phenomena

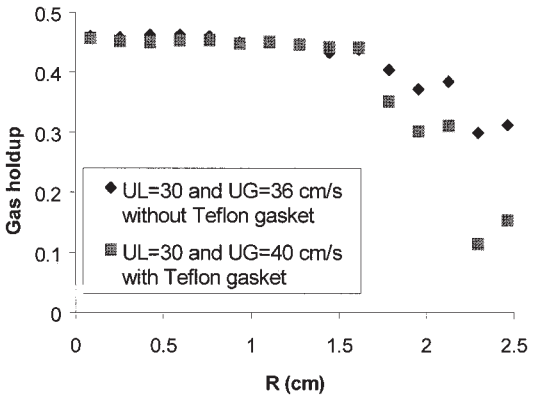

Figure 5. Comparison of azimuthally time averaged gas holdup radial profile without and with Teflon gasket.

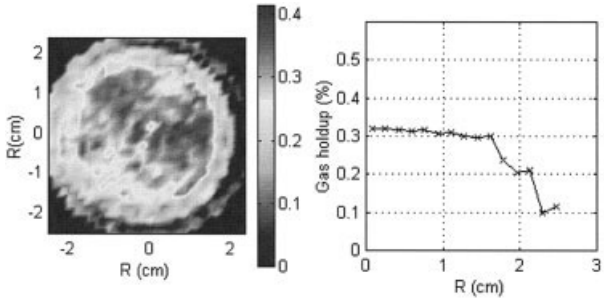

Figure 7. Gas holdup distribution at U_L= 0.5 m/s (Q_L = 7.7GPM) and U_G = 0.3 m/s (Q_G = 39.3SCFH).

(a) Time averaged cross-sectionally gas holdup distribution; (b) azimuthally time averaged gas holdup radial profile. The average gas holdup over the entire radius is 0.236, which is equivalent to gas saturation ($\varepsilon_g/(1-\varepsilon_s)$) of 0.38.

of gas holdup reduction in the outer portion of the cross section of the monolith are observed, which result from backmixing induced by the ring at the entrance. Similar findings were observed for the remaining flow conditions listed in Table 1. This indicates that the entrance and exit regions need to be carefully designed and should be free of any obstacles and vortex creating devices.

Mewes et al. (1999) and Kreutzer et al. (2003) reported that in the Taylor flow regime (slug flow regime), the ratio between the average velocity of the liquid slugs and the average velocity of bubbles is close to unity since the flow of liquid in the thin gravity-driven falling film between the bubble and the wall is very small. Thus, the average liquid holdup equals approximately the ratio of liquid flow rate (or the superficial liquid velocity) to the total flow rate (or the superficial velocities of the liquid and gas phases). However, Kreutzer et al. (2003) observed that the bubble excess velocity increases with the sum of gas and liquid superficial velocity in a single channel experiment. Hence, inside a monolith bed, the distributed liquid holdup would be equal to the flow ratios only if the liquid and gas flows are evenly distributed over the cross-section of the monolith bed and there is no relative slip between the phases. However, in practice, it is possible that this could not be achieved. In this work, the calculated gas fraction based on $U_G/(U_G + U_L)$ was compared to the measured cross sectional averaged gas saturation ($\varepsilon_g/(1-\varepsilon_s)$) (where $1-\varepsilon_s = 0.62$), and reasonable agreement was obtained (Figures 4, 6, 7, and 8).

Evaluation of the Degree of Flow Uniformity

As mentioned earlier, for CT reconstruction, the scanned cross-section is divided into two-dimensional pixels defined by the *ij* index (*i* is designated for the row, and *j* is designated for the column). Holdups are estimated in each pixel. Thus, the degree of flow uniformity is estimated by evaluating the standard deviation of the holdup distribution over a designated region of the monolith cross-section, based on area-weighted deviation as follows (Jiang, 2000; Marcandelli et al., 2000):

$$\sigma = \sqrt{\sum_i \sum_j \frac{a_{ij}}{a_{tot}} \left(\frac{\varepsilon_{ij} - \varepsilon_{avg}}{\varepsilon_{avg}} \right)^2} \tag{16}$$

where a_{ij} and ε_{ij} are the area and holdup of a particular pixel in the two-dimensional reconstructed scanned cross-section, respectively. a_{tot} is the total scanned cross-sectional area, and ε_{avg} is the cross-sectional averaged holdup. σ values are either zero for ideal uniform distribution or larger than zero, but less than

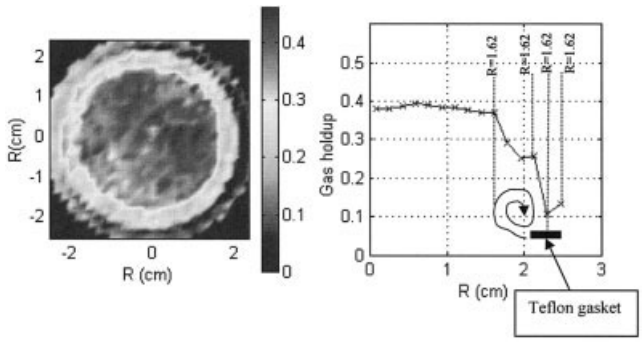

Figure 6. Gas holdup distribution at U_L = 0.4 m/s (Q_L = 6.2GPM) and U_G = 0.4 m/s (Q_G = 54.1SCFH).

(a) Time averaged cross-sectional holdup distribution; (b) azimuthally averaged gas holdup radial profile. The average gas holdup over the entire radius is 0.292, which is equivalent to gas saturation ($\varepsilon_g/(1-\varepsilon_s)$) of 0.471.

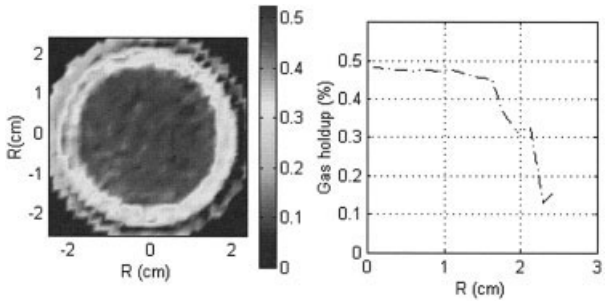

Figure 8. Gas holdup distribution at U_L = 0.3 m/s (Q_L = 4.6GPM) and U_G = 0.5 m/s (Q_G = 64.7SCFH).

(a) Time averaged cross-sectional gas holdup distribution; (b) azimuthally time averaged gas holdup radial profile. The average gas holdup over the entire radius is 0.366, which is equivalent to gas saturation ($\varepsilon_g/(1-\varepsilon_s)$) of 0.59.

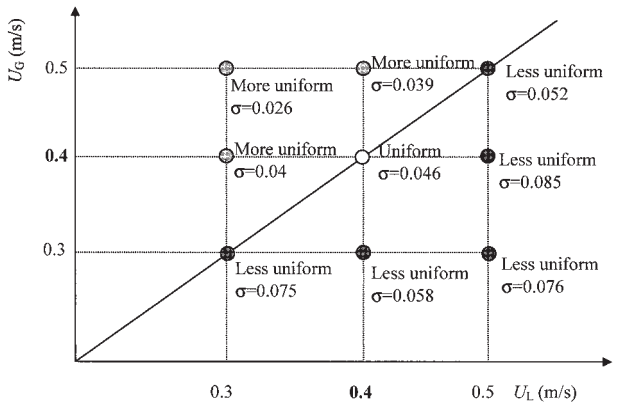

Figure 9. Qualitative evaluation of gas/liquid distribution uniformity in the monolith core $0 \leq R \leq 0.0162$ m (1.62cm) for the conditions studied.

1, based on the degree of flow uniformity. Lower values for the evaluated σ indicate more uniform flow.

Based on Eq. 11, σ is evaluated for the effective cross section of the monolith (i.e., $0 \leq R \leq 0.0162$ m (1.62cm)), shown in Figure 4 at all the liquid and gas flow rates used in this study. Figure 9 shows qualitatively the gas-liquid flow uniformity in the monolith $0 \leq R \leq 0.0162$ m (1.62cm) for the desired commercial flow conditions ($U_L = U_G = 0.4$m/s) and for all the conditions used that are bracketing this operating point. It can be seen that σ values vary between 0.026 and 0.085, which indicates that the gas-liquid distribution in the designated core region $0 \leq R \leq 0.0162$ m (1.62cm) is fairly uniform. However, if we designate uniform distribution for the desired commercial flow conditions ($\sigma = 0.046$), the distributions at the other flow conditions are defined as either less uniform if $\sigma > 0.046$ or more uniform if $\sigma < 0.046$.

According to Figure 9, with the distribution system used in this study, conclusions can be drawn as follows:

(i) At low superficial gas velocity ($U_G = 0.3$ m/s), the gas/liquid distribution is less uniform for all the superficial liquid velocities used (0.3, 0.4, and 0.5 m/s) .

(ii) At $U_L = 0.3$ m/s, gas/liquid distribution uniformity improves steadily once U_G is higher than 0.3 m/s. Higher U_G helps distribute the gas/liquid phase more uniformly at the entrance of the monolith.

(iii) At $U_L = 0.4$ m/s (the desired commercial flow conditions), gas/liquid distribution is designated to be uniform. The uniformity improves as U_G increases and worsens as U_G decreases (as in (ii) above).

(iv) At $U_L = 0.5$ m/s, gas/liquid distribution is less uniform than that obtained at the desired commercial flow conditions at all superficial gas velocities. It is evident that, as the liquid velocity increases, the gas/liquid phase distribution at the monolith entrance becomes less uniform. This is probably due to the effect of the monolith entrance and exit regions.

Remarks

In this study, it was shown that CT can readily estimate the bed average porosity. Further, CT can distinguish gross maldistribution in the monolith packing, as was verified by measuring the holdup distribution where part of the monolith was artificially flooded with liquid. This technique was then used to quantify the phase maldistribution at flow conditions specified for commercial reactor operation and at flow rates bracketing such conditions. Maldistribution of air and water due to wall effects at the monolith entrance was observed, and CT quantified these phenomena. Due to such maldistribution, the distributed holdups inside the monolith bed could not be determined by the flow ratios. However, a reasonable agreement was obtained between the gas fraction obtained based on flow ratios and the measured cross-sectionally averaged gas saturation at the studied conditions. The findings of this study imply that the entrance and exit regions of the monolith bed need to be carefully designed and to be free of obstacles and vortex creating devices. However, in the monolith core region, fairly uniform flow distribution was obtained for all the flow conditions used, which is quantified by the standard deviation of the holdup distribution evaluated in the monolith core region.

Acknowledgments

The financial support provided by Air Products and Chemicals, Inc., which made this work possible, is gratefully acknowledged. The help provided by Shaibal Roy in preparation of this manuscript is appreciated

Literature Cited

Albers, R. E., M. Nystrom, M. Siverstrom, A. Sellin, A.-C. Dellve, U. Andersson, W. Herrmann, and Th. Berglin, "Development of a Monolith-Based Process for H_2O_2 Production: From Idea to Large Scale Implementation," *Catalysis Today*, **69**, 247 (2001).

Beretta, A., E. Tronconi, and G. Forzatti, "Monolithic Catalyst for the Selective Reduction of NOx with NH3," *Structured Catalyst and Reactors*, A. Cybulski and J. A. Moulijn, eds., Marcel Dekker Inc., New York (1998)..

Boyer, C., and B. Fanget, "Measurement of Liquid Flow Distribution in Trickle Bed Reactor of Large Diameter with a New Gamma-Ray Tomographic System," *Chem. Eng. Science*, **57**, 1079 (2002).

Chen, J., R. Novica, M. H. Al-Dahhan, and M. P. Dudukovic, "Study of Particle Motion in Packed/Ebullated Beds by Computed Tomography (CT) and Computer Automated Radioactive Particle Tracking (CARPT)," *AIChE J.* **47**(5), 994 (2001).

Cybulski, A., and J. A. Moulijn, eds., *Structured Catalyst and Reactors*, Marcel Dekker Inc., New York (1998).

Cybulski, A., A. Stankiewicz, R. K. Albers, J. A. Edvinsson Moulijn, "Monolithic Reactors for Fine Chemicals Industries: A Comparative Analysis of a Monolithic Reactor and a Mechanically Agitated Slurry Reactor," *Chem. Eng. Science*, **54**, 2351 (1999).

Gulati, S. T., "Ceramic Catalyst Supports for Gasoline Fuel," *Structured Catalyst and Reactors*, A. Cybulski and J. A. Moulijn, eds., Marcel Dekker Inc., New York (1998).

Harter, I., C. Boyer, L. Raynal, G. Ferschneider, and T. Gauthier, "Flow Distribution Studies Applied to Deep Hydro-Desulfurization," *Industrial & Engineering Chemistry Research*. **40**(23), 5262 (2001).

Heibel, A. K., T. W. Scheenen, J. J. Heiszwolf, H. Van As, F. Kapteijn, and J. A. Moulijn, "Gas and Liquid Phase Distribution and Their Effect on Reactor Performance in the Monolith Film Flow Reactor," *Chem. Eng. Sci*, **56**, 5935 (2001).

Irandoust, S., and B. Andersson, "Liquid Film in Taylor Flow through a Capillary," *Ind. Eng. Chem. Res.* **28**(11), 1684 (1989).

Jiang, Y., *Flow Distribution and Its Impact on Performance of Packed-Bed Reactors*, PhD Thesis, Washington University, Missouri (2000).

Kreutzer, M. T., W. Wei, F. Kapteijn, J. A. Moulijn, and J. Heiszwolf, "Pressure Drop of Taylor Flow in Capillaries: Impact of Slug Length," 1st International Conference on Microchannels and Minichannels, Rochester, NY, USA, (2003).

Krishna, R., "Reactive Separation: A New Paradigm in an Old Bottle," Report from Chemical Engineering Department, University of Amsterdam (1999).

Krishna, R., "Reactive Separations: More Ways to Skin a Cat," *Chem. Eng. Science*. **57**(9), 1491 (2002).

Kumar, S. B., "Computed Tomography Measurements of Void Fraction and Modeling of the Flow in Bubble Columns," PhD Thesis, Florida Atlantic University (1994).
Kumar, S. B., M. P. Dudukovic, J. Chaouki, F. Larachi, and M. P. Dudukovic, "Computer Assisted Gamma and X-Ray Tomography: Applications to Multiphase Flow Systems," *Non-Invasive Monit. Multiphase Flows*, Elsevier, St. Louis, MO, p. 47 (1997a).
Kumar, S. B, M. P. Dudukovic, B. A. Toseland, J. Chaouki, F. Larachi, and M. P. Dudukovic, "Measurement Techniques for Local and Global Fluid Dynamic Quantities in Two and Three Phase Systems," *Non-Invasive Monit. Multiphase Flows*, Elsevier, St. Louis, MO, p. 1 (1997b).
Kumar, S. B., D. Moslemian, and M. P. Dudukovic, "A γ-ray Tomographic Scanner for Imaging Voidage Distribution in Two-Phase Flow Systems," *Flow Meas. Instrum*, **6**(1), 61 (1995).
Liu, W., "Ministructured Catalyst Bed for Gas-Liquid-Solid Multiphase Catalytic Reaction," *AIChE Journal*. **48**(7), 1519 (2002).
Liu, W., W. P. Addiego, C. M. Sorensen, and T. Boger, "Monolith Reactor for the Dehydrogenation of Ethylbenzene to Styrene," *Industrial & Engineering Chemistry Research*. **41**(13), 3131 (2002).
Lutran, P. G., K. M. Ng, and E. P. Delikat, "Liquid Distribution in Trickle Beds. An Experimental Study Using Computed-Assisted Tomography," *Ind. Eng. Chem. Res*. **30**(6), 1270 (1991).
Mantle, M. D., A. J. Sederman, L. F. Gladden, S. Raymahasay, J. M. Winterbottom, and E. H. Stitt, "Dynamic MRI Visualization of Two-Phase Flow in a Ceramic Monolith," *AIChE J*. **48**(4), 909 (2002).
Marcandelli, C., A. S. Lamine, J. R. Bernard, and G. Wild, "Liquid Distribution in Trickle-Bed Reactor," *Oil & Gas Science and Technology-Rev IFP*. **55**(4), 407 (2000).
Marchot, P., D. Toye, A.-M. Pelsser, M. Crine, and G. L'Homme, "Liquid Distribution Images on Structured Packing by X-Ray Computed Tomography," *AIChE J*. **47**(6), 1471 (2001).
Mazzarino, I., and G. Baldi, "Liquid-Phase Hydrogenation on a Monolithic Catalyst," *Recent Trends in Chemical Reaction Engineering*, Vol. II, B. D. Kulkarni, R. A. Mashelkar, M. M. Sharma, eds., Wiley Eastern Ltd., New Delhi, p. 181 (1987).
Mewes, D, T. Loser, and M. Millies, "Modelling of Two-Phase Flow in Packings and Monoliths," *Chem. Eng. Science*. **54**(21), 4729 (1999).
Nijhuis, X., M. T. Kreutzer, F. Kapteijn, and J. A. Moulijn, "Monoliths as More Efficient Three-Phase Reactors," presented in NASCRE-1, January 2001.
Pattrick, T. A., and M. A. Abraham, "Evaluation of a Monolith-Supported Pt/Al2O3 Catalyst for Wet Oxidation of Carbohydrate-Containing Waste Streams," *Environ Sci Techol*, 34 (2000).
Podrebarac, G. G., F. T. T. Ng, and G. L. Rempel, "The Production of Diaceton Alcohol with Catalytic Distillation: Part II. A Rate-Based Catalytic Distillation Model for the Reaction Zone," *Chem. Eng. Sci*, **53**(3), 1077 (1998).
Rammohan, A., "Characterization of Single and Multiphase Flows in Stirred Tank Reactors," PhD Thesis, Washington University, St. Louis (2002).
Reinecke, N., and D. Mewes, "Flow Regimes of Two Phase Flow in Monolith Catalyst," World Congress on Chemical Engineering, San Diego, CA (1996).
Reinecke, N., G. Petritsch, D. Schmitz, and D. Mewes, "Tomographic Measurement Techniques—Visualization of Multiphase Flows," *Chem. Eng. Technol*., **21**(7) (1998).
Roy, S., A. K. Heibel, W. Liu, and T. Boger, "Design of Monolithic Catalysts for Multiphase Reactions," Oral Presentation, 17th ISCRE (2002).
Schmit, C. E., D. Cartmel, and R. B. Eldridge, "Process Tomography: An Option for the Enhancement of Packed Vapor-Liquid Contactor Model Development," *Ind. Eng. Chem. Res*, **39**, 1546 (2000).
Schmit, C. E, D. Cartmel, and R. B. Eldridge, "The Experimental Application of X-Ray Tomography to a Vapor-Liquid Contactor," *Chem. Eng. Sci*, 56, 3431 (2001).
Stankiewicz, A. and J. A. Moulijn, "Process Intensification: Transforming Chemical Engineering," *Chem. Eng. Prog., 96, 22 (2000).*
Stankiewicz, A., "Process Intensification in In-line Monolithic Reactor," *Chem. Eng. Science*, **56**, 359 (2001).
Toye, D., P. Marchot, M. Crine, M. Pelsser, and G. L'Homme, "Local Measurements of Void Fraction and Liquid Holdup in Packed Columns Using X-Ray Computed Tomography," *Chem. Engineering and Processing*, **37**(6), 511 (1998).
Wang, Z., A. Afacan, K. Nandakumar, and K. T. Chuang, "Porosity Distribution in Random Packed Columns by Gamma Ray Tomography," *Chem. Engineering and Processing*, **40**, 209 (2001).
Yin, F., A. Afacan, K. Nandakumar, and K. T. Chuang, "Liquid Holdup Distribution in Packed Columns: Gamma Ray Tomography and CFD Simulation," *Chem. Engineering and Processing*, **41**, 473 (2002).

Manuscript received Apr. 21, 2004, and revision received July 12, 2005.